CHAPTER 6

DESIGN, ANALYSIS AND SIMULATION OF STAGGER TUNED GYRO-TWYSTRON

6.1. Introduction

In Chapter 5, a performance improvement study of a two-cavity PDL gyro-twystron is discussed. An intermediate cavity is added to a single cavity PDL gyro-twystron to increase gain and efficiency. Recent advances in radar applications have focused on gyro amplifiers that produce high RF peak power and operate in *Ka*-band and *W*-band. However, advanced high-resolution imaging radar applications require more versatile tubes that operate at a stable, high power, and wide bandwidth. According to extensive literature reviews, gyro-twystron is a viable candidate for use in millimeter-wave high-resolution radar applications. The output portion part of the gyro-twystron uses smooth wall waveguides, which can operate over a large frequency range, the gyro-twystron bandwidth is primarily limited by the quality factor of the pre-bunching cavities. To avoid this limitation and widen the bandwidth of the gyro-twystron, one can go for the designed cavities that resonate at slightly different frequencies, similar to conventional klystrons, and are placed between the input cavity and the output waveguide. This bandwidth enhancement technique, called stagger-tuning, initiated in klystron, is employed in gyro-twystron to enhance the bandwidth [152].

The effect of stagger-tuning on the performance of gyro amplifiers has been reported in the literature by many authors [114-120]. In 1999, Calem *et al*. experimentally investigated 35 GHz three-cavity gyroklystron stagger tuning of the input and buncher cavities with respect to the center frequency and width of the output cavity resonance [71]. Garven *et al*., in the year 2000, reported stagger-tuned four cavities, *Ka*-band gyro klystron amplifier [72]. A four-cavity W-band gyro klystron amplifier was developed, generating an output power of 67 kW, an efficiency of 28%, and a corresponding gain of 0.50% [73]. Linear and nonlinear theory of gyrotwystron

with stagger-tuned cavities has been analyzed and reported an effective enhancement in bandwidth reported [117], [118]. To obtain the higher bandwidth with moderate gain, Kou *et al.* proposed the stagger tuned (i.e., cavities resonant at different frequencies) *Ka*-band multi-cavity gyrotwystron amplifier [119].

In general, stagger-tuning enhances bandwidth while decreasing device gain. As a result, the trade-off in the gain-bandwidth product must be thoroughly examined for the device to work optimally, because the gain-bandwidth product is a key measure for characterizing an amplifier's performance. As a result, the influence of stagger-tuning on the bandwidth, gain, and gain-bandwidth product of the designed gyro-twystron amplifier has been thoroughly investigated in this chapter.

In the present work, to improve the bandwidth of a multi cavity gyro-twystron, a stagger tuned, cavities where the electron beam of high beam velocity ratio (>1) are amplified is proposed. The behavior of a beam-wave interaction in multi cavity gyrotwystron amplifier was investigated using self-consistent nonlinear theory and verified using a 3D particle-in-cell (PIC) simulation code. Moreover, the subassemblies, including a double anode MIG, a three stage depressed collector, and a dielectric Meta surface output window, were designed and studied in detail. In section 6. 2, self-consistent nonlinear analysis is disused. Section 6. 3, discusses the double anode magnetron injection gun (MIG). Design and modelling of RF interaction circuit of multi cavity gyrotwystron amplifier, three stage depressed collector, and dielectric Meta surface output window simulation results addressed in section 6. 4. in section 6. 5, conclusions are made.

6.2. Nonlinear Analysis of Stagger Tuned Gyro-Twystron

A nonlinear analytical analysis [100] is used to investigate the impact of stagger-tuning on the gyro-twystron amplifier. This study is based on a technique utilized before

in formulating the idea of the stagger-tuned gyroklystron. The subsequent sections discuss the process of electron prebunching in staggered tuned cavities and the interaction mechanism between gyrating electron beam and wave in a waveguide of a gyro-twystron.

6.2.1. Pre Bunching Section

The way electrons bunch up in stagger-tuned cavities that are separated by drift regions can be shown by the following equations [117], [118], [153]:

$$\frac{dw}{d\zeta} = -2(1-w)^{s/2}\,\mathrm{Re}(F_n f_n e^{-n\theta}) \tag{6.1}$$

$$\frac{d\theta}{d\zeta} = w - \Delta' + s(1-w)^{s/2-1}\,\mathrm{Im}(F_n f_n e^{-n\theta} \tag{6.2}$$

The index n denotes an n^{th} cavity, while the function f_n denotes the axial structure of the n^{th} cavity field. where $\theta = s\Theta - \omega t$, $\zeta = \beta_{\perp 0}^2 / 2\beta_{\|0}\,(\omega z/c)$ is normalized axial coordinate, $\Delta' = \left(2/\beta_{\perp 0}^2\right)(1 - s\Omega_0/\omega)$ is cyclotron resonance mismatch, $F = (eA/m_0\Omega_0\gamma_0)(s/2)^{s-1}(\beta_{\perp 0}^{s-4}/(s-1)!)J_{m\pm s}(k_\perp R_0)e^{-n(m\pm s)\psi}$ is normalized field amplitude at the cavity end.

One can determine the electron beam's sensitivity to the n^{th} cavity resonant field by integrating (6.1) and (6.2).

$$\chi_n = \frac{-2n}{sF_n}\left[\frac{1}{2\pi}\int_0^{2\pi}\left(\int_0^{\zeta_{n,c}}(1-w)^{s/2}\,f_n(\zeta)e^{n\theta}d\zeta\right)d\theta_0\right] \tag{6.3}$$

where $\zeta_{n,c} = \left(\beta_{\perp 0}^2/2\beta_{\|0}\right).(\omega L/c)$ is normalized cavity length, θ_0 is the initial gyro phase uniformly distributed between zero and 2π at the first cavity's entrance. The impact of significant phase bunching in lengthy drift sections can be described by this phase. This susceptibility acts as a source term in the above equations that describe the excitation of electromagnetic fields in cavities.

Excitation of the field in the input cavity can be explained as follows

$$\left|F_1\right|^2 = \frac{A_{sig}^2}{\left(1-I_{c,1}\chi_1^{"}\right)^2+\left(\delta_1+I_{c,1}\chi_1^{'}\right)^2} \tag{6.4}$$

$$\tan\psi_1 = \frac{\delta_1+I_{c,1}\chi_1^{'}}{1-I_{c,1}\chi_1^{"}} \tag{6.5}$$

The complex amplitude F_1 is shown here as $\left|F_1\right|e^{n\psi_1}$, $A_{sig}^2 = \dfrac{4I_{c,1}P_{in}Q_1}{p_{0\perp}Q_{cpl}}$ is the normalized intensity of the field excited by input signal in the input cavity and is related to the input power P_{in}. Where Q_{cpl} coupling or external quality factor of the input cavity, $P_{0\perp} = \left[\beta_{\perp 0}^2 \big/ 2\left(1-\gamma_0^{-1}\right)\right]V_b I_b$ is the beam power related to the gyrating electron, V_b and I_b are the beam voltage and beam current, respectively.

Since the present investigation is focused on the bandwidth characteristics of the gyrotwystron alone, we'll make the assumption that the input power and, thus, A_{sig}^2 be frequency-independent. The frequency detuning factor $\delta_1 = 2Q\left(\omega-\omega_1\right)/\omega$ is used in (6.4) to explain how the amplitude of the first cavity field varies with frequency. Here ω is the operating frequency, ω_1 is resonating frequency of the cavity, Q is quality factor of the input cavity. Similarly for i^{th} cavity $\delta_n = \dfrac{2Q_n(\omega-\omega_n)}{\omega}$

For all other cavities

$$\left|F_n\right|^2 = \frac{4I_{c,n}^2\left|u_n\right|^2\left|H_n\right|^2}{\left(I_{c,n}\chi_n^{"}-1\right)^2+\left(I_{c,n}\chi_n^{'}+\delta_n\right)^2} \tag{6.6}$$

$$\tan\psi_n = \frac{\delta_n+I_{c,n}\chi_n^{'}}{1-I_{c,n}\chi_n^{"}} \tag{6.7}$$

When the cavities are sufficiently short, the field amplitude and phase of the resonant field are expressed as

$$\left|F_n\right|^2 = \frac{4I_{c,n}^{'2}\left|X_n^{'}\right|^2}{1+\delta_n^{'2}} \tag{6.8}$$

$$\tan\psi_n = \delta_n^{'} \tag{6.9}$$

where $\delta_n^{'} = \frac{\delta_n}{\left(1+I_{c,n}\right)}$, $I_{c,n}^{'} = \frac{I_{c,n}}{\left(1+I_{c,n}\right)}$

6.2.2. Output Waveguide

The interaction between the prebunched gyrating electron beam and electromagnetic waves in a waveguide is described by a self-consistent nonlinear equations [117], [117], [153] for the variations in normalized electron energy (w), phase (θ) and wave amplitude (F) along the axis of the RF circuit.

$$\frac{dw}{d\zeta} = -2\frac{(1-w)^{s/2}}{1-bw}\mathrm{Re}(Fe^{-n\theta}) \tag{6.10}$$

$$\frac{d\theta}{d\zeta} = \frac{1}{1-bw}\left[w-\nabla^{'}+s(1-w)^{(s/2)-1}\,\mathrm{Im}\left(Fe^{-n\theta}\right)\right] \tag{6.11}$$

$$\frac{dF}{d\zeta} = -I\frac{1}{2\pi}\int_0^{2\pi}\frac{(1-w)^{s/2}}{1-bw}e^{n\theta}d\theta_0 \tag{6.12}$$

Where $b = h\beta_{\perp 0}^2 \big/ 2\beta_{\|0}\left(1-h\beta_{\|0}\right)$ is the parameter responsible for variations in electron axial velocity during EM wave radiation (i.e. recoil effect), *h* is the normalized axial wavenumber. The efficiency of the gyrotwystron is defined as

$$\eta = \frac{\beta_{\perp 0}\eta_{\perp}}{2\left(1-\gamma_0^{-1}\right)\left(1-h\beta_{\|0}\right)} \tag{6.13}$$

where $\eta_{\perp} = \frac{1}{2\pi}\int_0^{2\pi} w\left(\zeta_{wg}\right)d\theta_0$ is the transverse efficiency and $w\left(\zeta_{wg}\right)$ is the normalized particle energy at the end of the output waveguide.

The output power of the gyro-twystron is defined in terms of wave intensity and other parameters as

$$P_{out} = \frac{p_{0\perp}\left|F\left(\zeta_{wg}\right)\right|^2}{I_0\left(1-h\beta_{\|0}\right)} \tag{6.14}$$

here the wave intensity $\left(\left|F\left(\zeta_{wg}\right)\right|^2\right)$ at the output waveguide end, which is considered to be significantly higher than the input wave's intensity. Using equation (6.10), (6.11), and (6.12) the amplifier's gain at the output end is defined as:

$$G = 10\log\left(\frac{\left|F\left(\zeta_{wg}\right)\right|^2}{A_{sig}^2}\right) + G_{const} \tag{6.15}$$

As, the field amplitude and phase are effectively depends on the stagger tuning parameter, defined as $\nabla' = \left(2/\beta_{\perp 0}^2\right)\left(\frac{\left(\omega_c - k_{\|0}\beta_{\|0} - s\Omega_0\right)}{\omega}\right)$, it will significantly alter the device outputs. This cyclotron resonance mismatch, control the bandwidth variation and this change in stagger tuned bandwidth $\left(BW_{\nabla'}\right)$ corresponding to the synchronous tuned bandwidth $\left(BW\right)$ is observed as: $BW_{\nabla'} = \left(\frac{2}{\beta_{\perp 0}^2}\right)BW$. The normalized gain-bandwidth product, an essential parameter required for any radar source is defined as the ratio of the gain-bandwidth product of stagger-tuned amplifier $\left(BW_{\nabla'} \times G_{\nabla'}\right)$ to that of non-stagger-tuned amplifier $\left(BW \times G\right)$, $\Phi = \frac{BW_{\nabla'} \times G_{\nabla'}}{BW \times G}$.

6.2.3. Gain and Bandwidth study of Stagger Tuned Gyro-Twystron

In the present design study [Fig. 6.1], the gyrating electron beam is modulated three times in three cavities; therefore, by selecting suitable parameters, the

performance of the gyrotwystron can be improve. The bunching factor at the output waveguide entrance can be depends on the initial bunching parameter, length of the drift region and normalized quality factors of cavity 1, cavity 2, cavity 3 respectively.

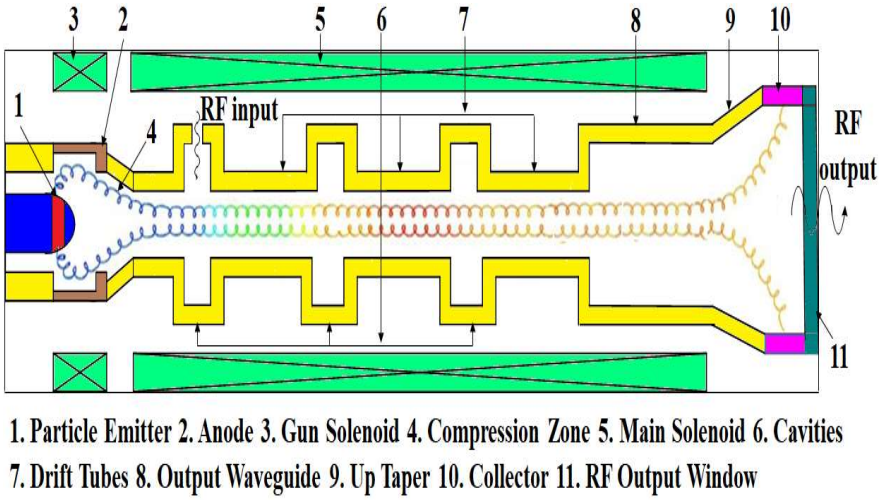

Fig. 6. 1. Schematic diagram of multi cavity gyrotwystron.

A three cavity prebunching gyrotwystron operating at the fundamental harmonic (s=1) with 70 kV, 10 A beam parameters, and beam velocity ratio of 1.4 is investigated to study its performance through its gain, bandwidth, and gain-bandwidth product. The bandwidth and efficiency depend on the bunching parameter (X_0) depicted in Fig. 6. 2. (a) and (b). The bandwidth reaches its maximum when the optimum value of X_0=0.2. After that value, the bandwidth decreases due to the occurrence of over bunching. Also, the efficiency is maximum (~ 48%). Generally, when all cavities operate at the same frequency (i.e., synchronous tuning), the device gain is maximum. Fig. 6. 3 shows the variation of gain degradation of stagger-tuned gyrotwystron as the function of a stagger-tuning parameter (∇). It is quite obvious and confirmed by Fig. 6. 3 (a) that the gain degradation increases with the stagger-tuning parameter while the overall gain of the device decreases due to frequency mismatch between the cavities of the gyrotwystron amplifier. The maximum gain degradation for the three cavity stagger-tuned

gyrotwystron is obtained at around 8 dB for the stagger tuned gyrotwystron as the function of the stagger-tuning parameter $(\nabla = 1)$. Fig. 6. 3 (b) shows the variation of normalized bandwidth of three cavities stagger-tuned gyrotwystron as the function of the stagger-tuning parameter (∇). It can be observed that the normalized bandwidth of the three cavity gyrotwystron amplifier increases by two times at $\nabla = 4$ as compared to the three cavity gyrotwystron amplifier without stagger-tuning. However, more bandwidth enhancement occurs at large values of ∇, where device operation is impractical because of substantial gain loss caused by stagger-tuning. Therefore, the

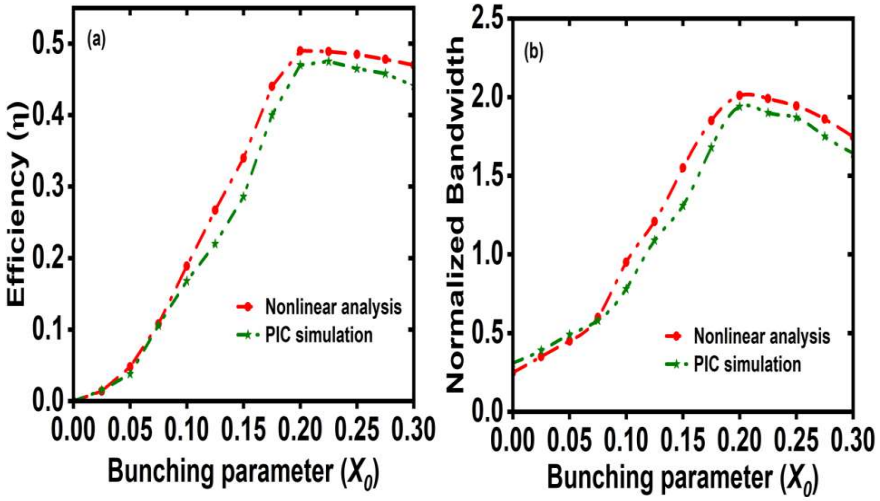

Fig. 6. 2. (a) Efficiency and **(b)** Normalized bandwidth versus bunching parameter.

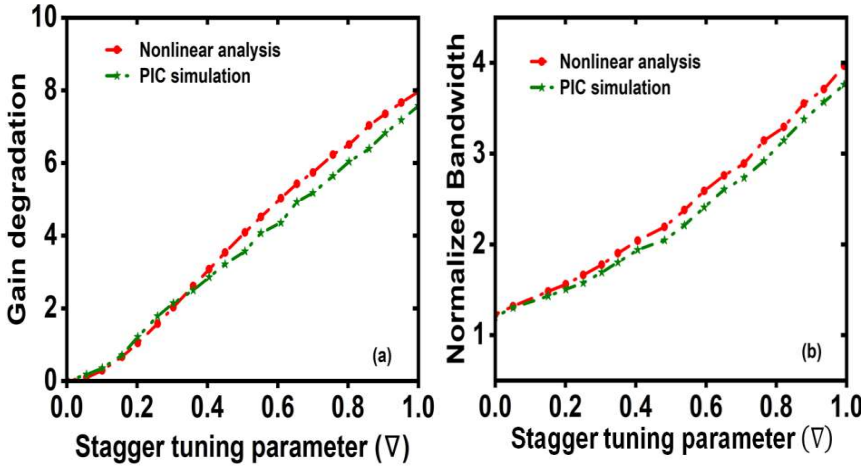

Fig. 6. 3. (a) Gain degradation and **(b)** normalized bandwidth versus stagger tuning parameter.

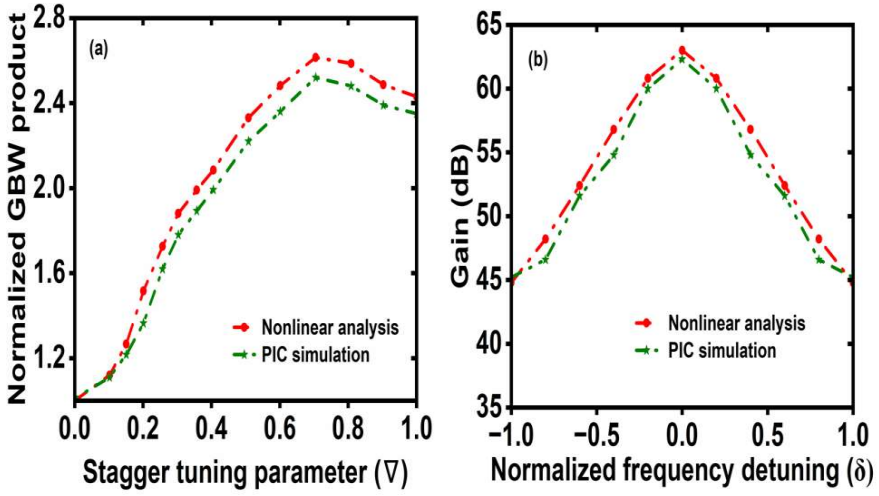

Fig. 6. 4. (a) Stagger tuning parameter versus normalized GBW product. (b) Gain versus normalized frequency detuning.

choice of stagger-tuning for the device should be determined as a result of a trade-off between the gain and bandwidth. Hence, the appropriate stagger-tuning parameter for the gyrotwystron should be chosen based on its maximum gain bandwidth product. The normalized gain-bandwidth product of the stagger-tuned gyrotwystron amplifier is obtained by nonlinear analysis has been validated against the PIC simulation, as illustrated in Fig. 6. 4. It can be seen from Fig. 6. 4 (a), the decline in normalized gain bandwidth product value above a particular value of stagger tuned parameter can be attributed to the substantial gain degradation of the device. Therefore, stagger-tuning in gyrotwystron amplifier should be done to a low extent, in order to have best possible performance of the device in terms of its gain-bandwidth product. The analytical observation of gain variation with regard to normalized frequency detuning is shown in Fig. 6. 4 (b), which is validated with simulation and found to be in close agreement.

6.3. Design of Double Anode Magnetron Injection Gun

A double anode magnetron injection gun is used for the current stagger-tuned multi-cavity gyrotwystron because this type of MIG offers an additional degree of freedom

(the voltage on the modulating anode) for fine-tuning the electron beam quality during operation. The mathematical trade-off equations [37] are used to compute the fundamental MIG design parameters, such as the emitter radius, cathode magnetic field, anode-cathode gap, and slant length. These design parameters' formalism remains the same, as discussed in Chapter 4. After acquiring the preliminary design parameters, a commercially available E-GUN code [127] is used to model and simulate the double anode MIG. Table 6.1 displays the fundamental design parameters and the simulation's results. Fig. 6. 5 displays the magnetic field profile, the electron beam trajectory, and the current MIG 2D structure. The magnetic field compression ratio is calculated as 12. The desired beam velocity ratio and velocity spread were calculated as 1.4 and ~2% using the post-processing program PPGYRO. The device's performance depends on the quality of the electron beam, and even minor deviations in MIG design parameters might have undesirable outcomes. Consequently, the study of the sensitivity of beam quality to operating conditions was investigated. Fig. 6. 6 shows the variation in velocity ratio and velocity spread corresponding to accelerating anode voltage and modulating anode voltage. As shown in Fig. 6. 6 (a), when the accelerating anode changes from 65 kV to 75 kV, the velocity ratio decreases because the axial velocity of the electron beam is directly dependent on the accelerating anode voltage. Fig. 6. 6 (b) shows the velocity ratio increases as modulating anode increases.

Table 6. 1 Design Parameters of Double Anode MIG

Parameters	**Value**
Beam current (I_b)	10 A
Beam voltage (V_b)	70 kW
Velocity ratio (α)	1.4
Magnetic Field	1.31T
Compression ratio (f_m)	12
Velocity spread	~2 %
Cathode Angle (θ)	40º

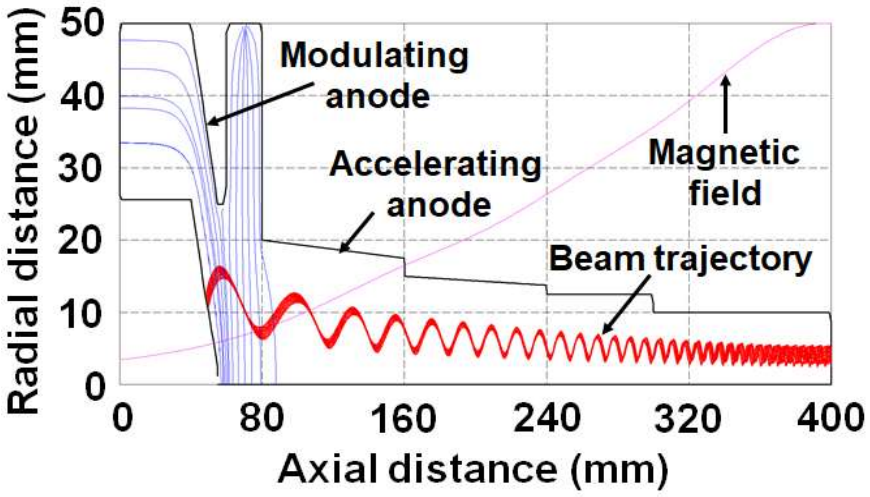

Fig. 6. 5. Electron beam trajectory, magnetic field, and equipotential lines of MIG.

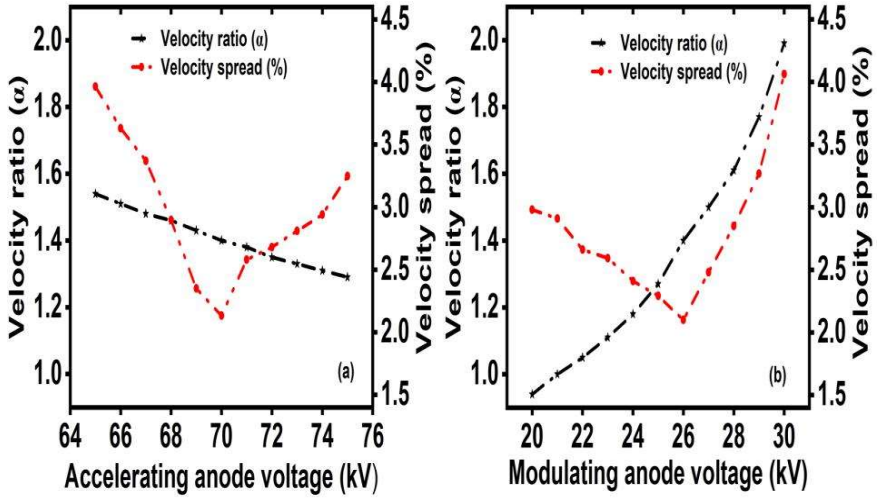

Fig. 6. 6. Parametric study of velocity ratio and velocity spread for **(a)** Accelerating anode voltage, **(b)** Modulating anode voltage.

6.4. Design and Modelling of RF Interaction Structure

6.4.1 Design of RF Interaction Circuit

The present millimeter wave gyro-twystron consists of three cylindrical cavities with radius r_c and length r_l, three drift tubes and an output cylindrical waveguide. The beam-wave interaction mechanism in a multi-cavity gyro-twystron can be divided into four stages: (1) in the input cavity, modulation occurs due to an externally applied cavity field. (2) In a drift tube, bunching processes occur without wave interaction. (3)

In the intermediate cavity, pre-bunched electrons form a steady-state cavity mode, and (4) in the waveguide, beam wave interaction take place. Cavities are designed with certain dimensions to resonate at the desired operating frequency and mode.

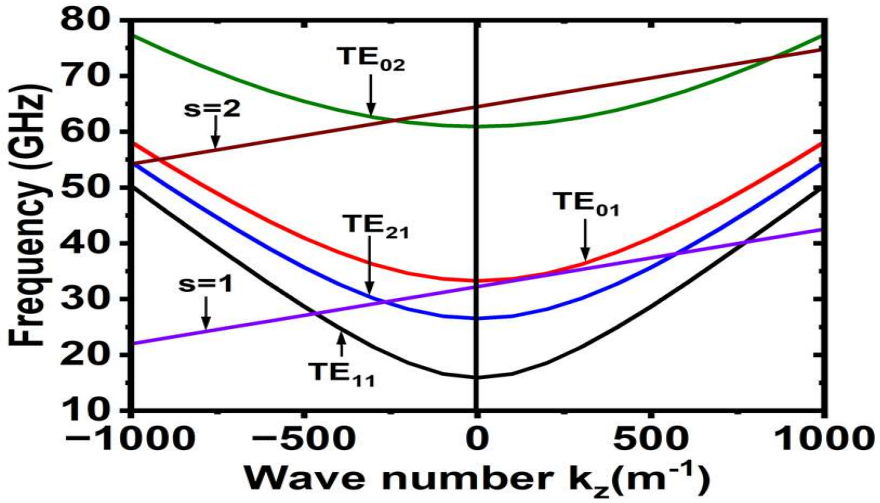

Fig. 6. 7. Dispersion diagram of multi cavity gyro-twystron.

To provide the cut-off to the TE_{01} mode and prevent field propagation, the drift region radius is selected such that to fulfil the condition $r_b < r_d < r_w$. The drift tube's length is computed using the cold cavity dispersion relation [29] in order to adequately separate the cavities and output waveguide. The operating characteristics and nature of beam wave interaction of gyro-twystron is discussed through the dispersion diagram, as shown in Fig. 6. 7 the diagram illustrates the fundamental cyclotron beam line intersection with the TE_{01} mode line in the positive k_z region at 35 GHz. The beam mode line also intersects with TE_{11} and TE_{21} modes (*i.e.* backward wave modes) in the negative k_z region. The beam current is chosen below the start oscillation current and the waveguide length is chosen to be smaller than the start oscillation length for the gyro-twystron to operate stably [119].

6.4.2 Modelling and Cold Simulation

The RF structure of three cavity gyro-twystron [Fig. 6. 8] is modeled using CST Microwave Studio [141] to study the RF propagation characteristic. The structural and electrical parameters are given in Table 6. 2. The walls of cavities, drift tubes, and waveguides are modelled using annealed copper. All cavities are operated in TE_{01} mode with the same length but varying radii to achieve distinct resonant frequencies. To obtain the desired quality factor for all cavities, dielectric rings are introduced at the end

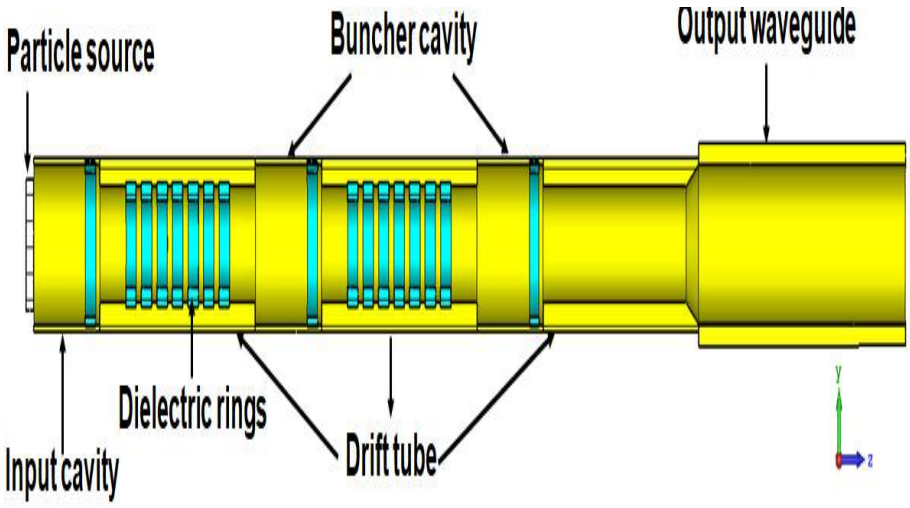

Fig. 6. 8. CST model of multi cavity gyrotwystron.

Table 6. 2 Design Parameters of Multi Cavity Gyro-Twystron

Parameters	**cavity**			**drift tube**			**Wave guide**
	1	**2**	**3**	**1**	**2**	**3**	
Radius (mm)	5.52	5.56	5.55	4	4	4	5.5
Length (mm)	12.8	12.8	12.8	30	30	30	50
Beam parameters	Voltage			Current			Pitch factor
	70 kV			10 A			1.4
Magnetic field	1.31 T						

end of each cavity. The drift tubes are modelled using design parameters to provide isolation between each cavity and output waveguide, and dielectric (AIN-SiC) loading

is employed in the drift region to provide a field-free environment within the drift tube. The output portion of the RF structure is a travelling waveguide is modelled with a 5.5 mm radius and a 40 mm length. For modelling the cathode in CST particle studio, a DC emission model of a circular particle source is chosen. The beam voltage of 70 kV is converted into a kinetic type velocity and the inverse tangent of 1.4 pitch factor is converted into angle of 54.5^0. In the present simulation, an electron beam with a voltage of 70 kV, a current of 10 A, a beam velocity pitch factor of 1.4 and a kinetic spread of ~ 2% are considered. In the absence of an electron beam (cold simulation), the cavities are simulated to identify the required operating frequency, mode and quality factor. The operating TE_{01} mode is confirmed by the maximum field midway between the wall and the center of the RF structure. The cold simulation predicted that all cavities operate in TE_{011} mode and are tuned to various resonant frequencies in order to attain a wider bandwidth via stagger tuning. The resonant frequency of the cavities is verified through post processing of the transient solver of CST MWS. The I^{st}, II^{nd} and III^{rd} cavities resonate at 34.890 GHz, 34.63 GHz and 34.76 GHz respectively. The corresponding quality factors for the first, second, and third cavities are 188, 194, and 194.

6.4.3 PIC Simulation and Validation

In the presence of electron beam (hot analysis) has been performed to explore the beam-wave interaction process using CST particle studio [141]. The PIC solver computes the particle dynamics in the presence of the field and calculates the field profile at short time intervals using a leapfrog scheme. The time step and accuracy in this self-consistent PIC simulation depend on the total number of mesh cells, which ultimately increases the simulation time and memory requirement. In the present simulation, Cells per wavelength were kept as 10 to provide better spatial sampling and accurate results. A circular particle source cathode is designed using a DC emission

model for particle emission. The cathode emits the electron beam with a voltage of 70 kV and the beam current of 10 A. Under a constant magnetic field of 1.31 Tesla, the gyrating electron beam with a beam velocity pitch factor of 1.4 and ~2% kinetic spread enters into the input cavity, where the electron beam interacts with the externally applied RF input signal of 0.25 Watts and gets modulated. These modulated electrons form a bunch in the drift tube. The bunched electrons move towards the non-resonant output waveguide, where bunched electrons interact with the RF wave and transfer its kinetic energy to the wave, hence amplifying the RF signal. Fig. 6. 9 depicts the amplified RF signal at the output port in TE_{01} mode corresponding the simulation duration. The maximum E-field strength generated in TE_{01} mode at the output port. Fig. 6. 10 (a) shows the RF output power at the waveguide output port for the TE_{01} operating mode. An instantaneous power of ~600 kW or an average over an RF period of actual radiated output power achieves a maximum value of ~300 kW for 0.25 W input power with efficiency of ~43 %, gain of ~60 dB, and bandwidth ~2.8 GHz. These results are compare with the *Ka*-band gyro-twystron reported by Kou et al. [119] is given in table 6.3.

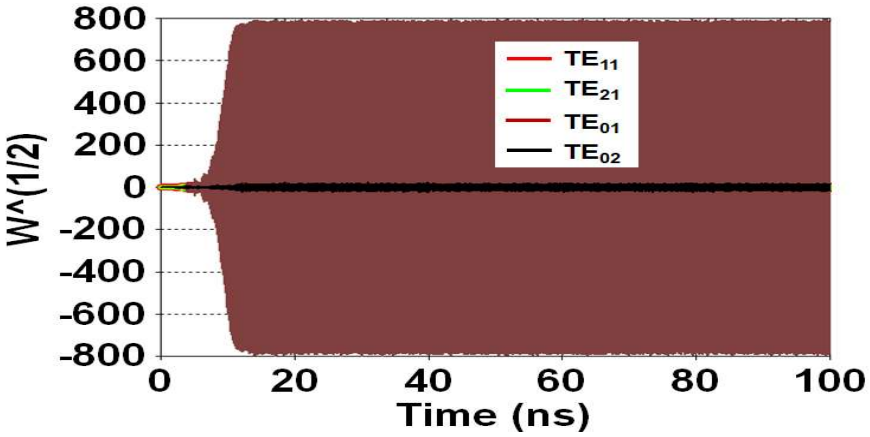

Fig. 6. 9. Temporal growth of E-field in desired operating TE_{01} mode and TE_{11}, TE_{21}, TE_{02} modes.

Table 6. 3 Comparision of *ka*-band gyro-twystron amplifier

Device	Output Power	Gain	Efficiency	Bandwidth
Ka-band 3- cavity gyrotwystron by C. S. Kou *et al* [119]	80 kW	55 dB	33%	0.7 GHz
Present gyrotwystron amplifier	300 kW	60 dB	43 %	2.8 GHz

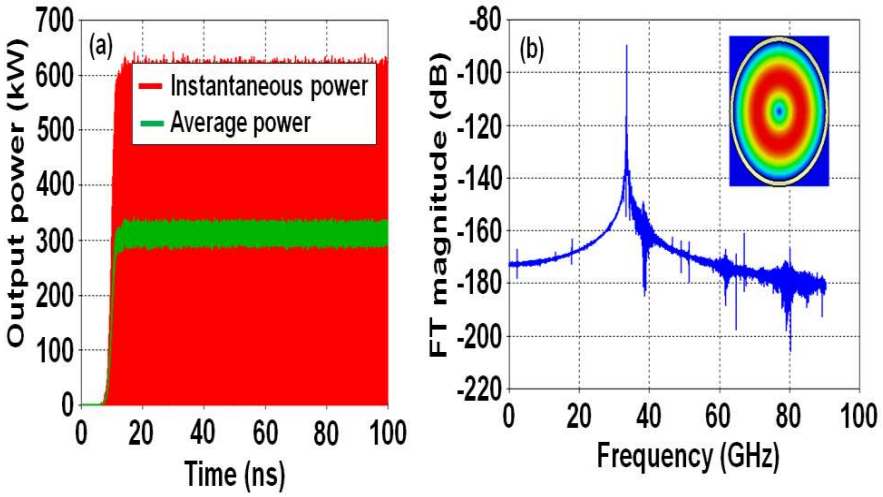

Fig. 6. 10. (a) Output signal at port two and **(b)** FT signal with contour plot (inset).

Fig. 6. 10 (b) shows that output power is developed at 35 GHz and the contour plot confirmed the desired operating TE_{01} mode. The simulated amplifier performance is validated using the self-consistent nonlinear theory, as shown in Fig. 6. 11, and it is observed that both are in good agreement with 2%.

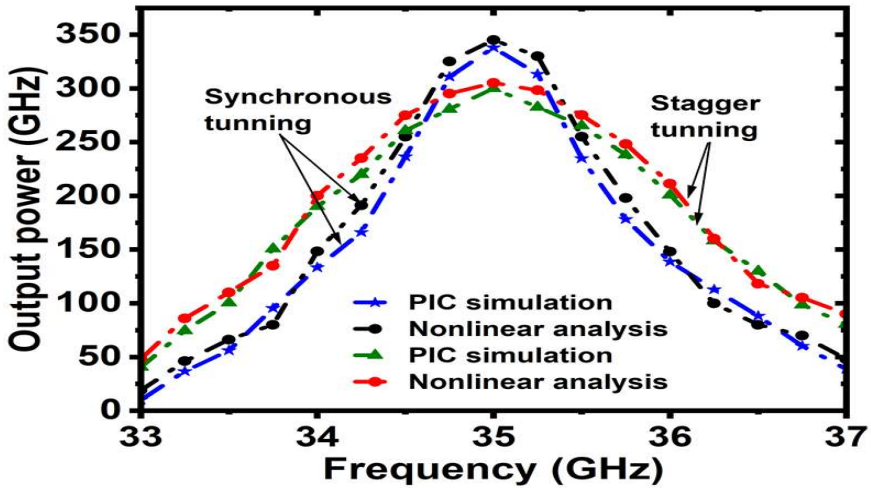

Fig. 6. 11. Comparision of synchronous tuning and stagger tuning.

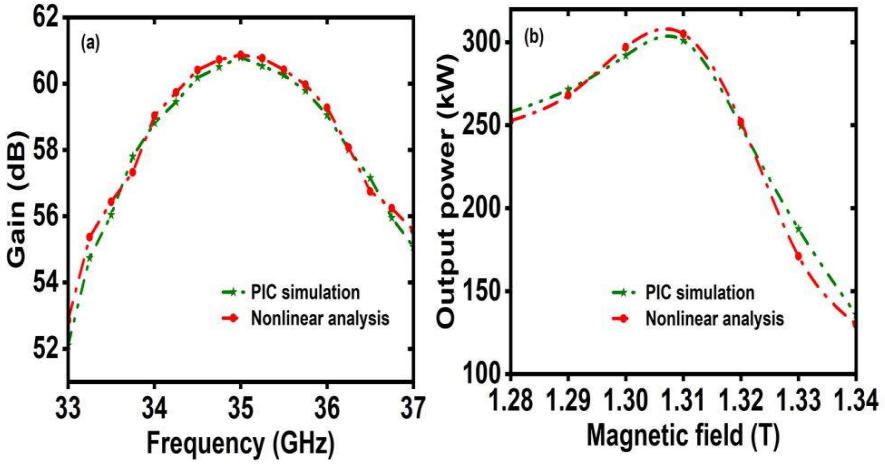

Fig. 6. 12. Comparision of PIC simulation and nonlinear analysis **(a)** Frequrncy versus Gain **(b)** Magnetic field versus Output power.

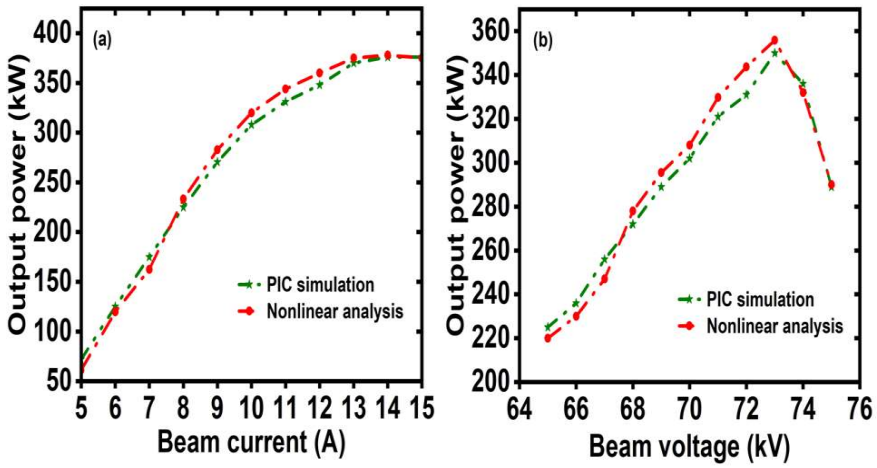

Fig. 6. 13. (a) Beam current versus Output power, **(b)** Beam voltage vrsus Output power.

Further, current stagger-tuned gyrotwystron simulation and nonlinear analysis results are compared with the without stagger tuned gyrotwystron amplifier [Fig. 6. 11]. This study demonstrates that the bandwidth enhancement of the stagger-tuned gyrotwystron is two times greater than that of the without stagger tuned gyrotwystron.

In addition, the performance of the current stagger-tuned gyro-twystron is investigated by estimating the gain for different frequencies using nonlinear theory and PIC simulation [Figure 6. 12 (a)]. The impact of the applied magnetic field has been studied. The maximum power at the operating dc magnetic field 1.31 T [Fig. 6. 12 (b)],

which effectively synchronizes the gyrating beam's velocity with the electromagnetic field. The effect of the beam current on output power as shown in Fig. 6. 13 (a). As can be seen in Fig. 6. 13 (b), the applied dc voltage affects the properties of the gyrating beam, which impacts the interaction between the beam and wave.

6.5. Design of Output System

6.5.1 Three Stage Depressed Collector

The efficiency of any microwave vacuum tubes should be as high as possible. A multi-stage depressed collector [Fig. 6.14] is employed as a recovery system to recover the energy from the spent electron beam [154], which is lost as heat in the collector region, in order to increase the total device efficiency. In depressed collector, depressed potential is applied at the collector electrode and electron energy is recovered via the

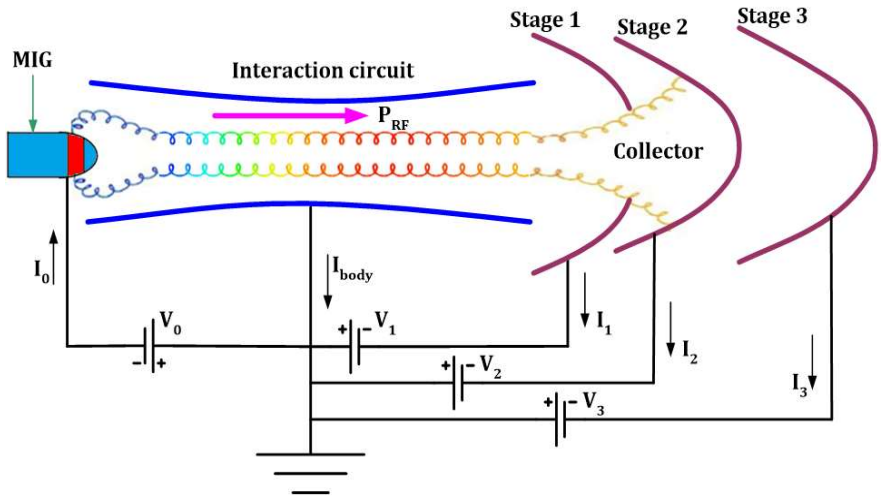

Fig. 6. 14. Scematic diagram of gyro device with multi stage depressed collector.

loop current. The beam energy collected at the collector's electrodes can be computed as follows:

$$P_{col} = \sum_i V_i I_i \tag{6.16}$$

where i is number of stages, V_i and I_i are the potential and collected beam current at the i^{th} stage electrode. Increasing the number of stages enhances the efficiency of the depressed collector but increases the design's complexity. The depressed collector efficiency is defined as

$$\eta_{col} = P_{col} / P_{spent-beam} \tag{6.17}$$

The total efficiency of the present gyro-twystron amplifier is improved after the depressed collector is introduced and can be defined as [23],

$$\eta_{total} = \frac{P_{out}}{P_{DC} - P_{col}} = \frac{\eta_e}{1 - \eta_{col}\left(1 - \eta_e\right)} \tag{6.18}$$

where P_{out}, P_{DC}, and P_{col} are RF output power, beam power, and spent beam power collected at depressed collector surface, η_e electronic efficiency of the device. Using the electron trajectory code EGUN [127], a three-stage depressed collector for *Ka*-band gyro-twystron is designed. For the EGUN simulation, the electron beam information is obtained from the gyro-twystron PIC simulation. In the present design, assumed that all electrons are collected on the electrodes without considering secondary emission. The minimum electrode potential was selected as the minimum energy of electrons to prevent backstreaming. The maximum potential was selected as the operating beam voltage. Fig. 6. 15 depicts the beam trajectories in the three stage depressed collector. Table 6. 3 displays the collector efficiency for each stage in terms of optimum electrode potential. Gyro-twystron total efficiency increases from ~ 43% to ~78% when combined with the three-stage depressed collector's ~ 80% collector efficiency.

Table 6. 4 Collector Efficiency for Different Stages

Stage	**Potential on electrodes (kV) (relative to the ground potential)**			**Collector Efficiency**
1	- 23.5	…	…	42.8%
2	- 23.5	- 48.0	…	69%
3	- 23.5	-48.0	-70	80%

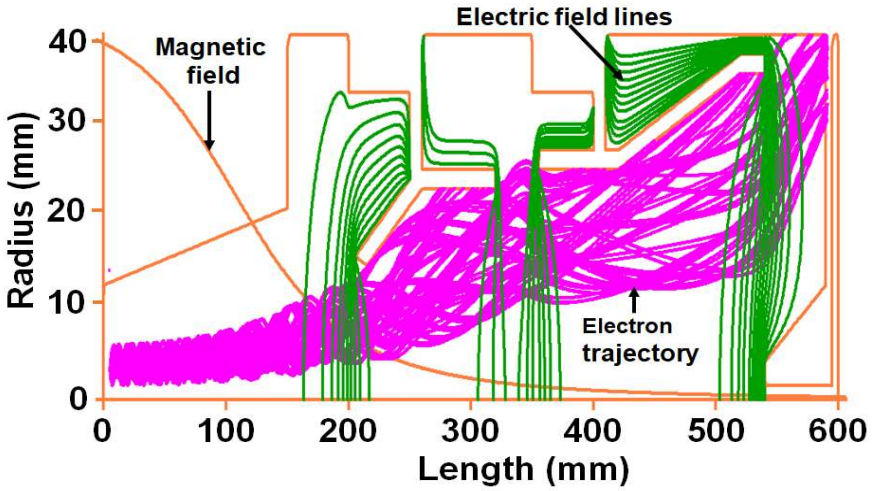

Fig. 6. 15. Electron beam trajectory in three stage depressed collector

6.5.2 Meta Surface RF Output Window

RF output window is an essential component of vacuum electron devices. The RF output window must be transparent to RF and opaque to the atmosphere. From an RF point of view, the RF output windows should have minimal reflection and high transmission. In order to overcome the drawbacks of multilayer windows [155], in the present design, a meta-surface output window is used for broad bandwidth.

A window is modelled in CST using a BeO (beryllium oxide) (ε_r = 6.7) flat dielectric disk as the base structure. Square pillars are placed periodically on both sides of flat dielectric disc surfaces. The base dielectric disc has a radius and thickness of r=16 mm and t =3.4 mm, respectively. The height and width of pillars are h =2.7 mm, w= 2.2 mm, and the distance between adjacent pillars is g =0.5 mm. So, the period is w + g. According to the multilayer matching principle [155], the best equivalent permittivity for meta-surface matching layers can be found as $\varepsilon_r = \sqrt{\varepsilon_r} = 2.5$. By optimizing the lattice dimensions w and g, to get the impedance match between the guide and the base dielectric disk, and a wideband window response.

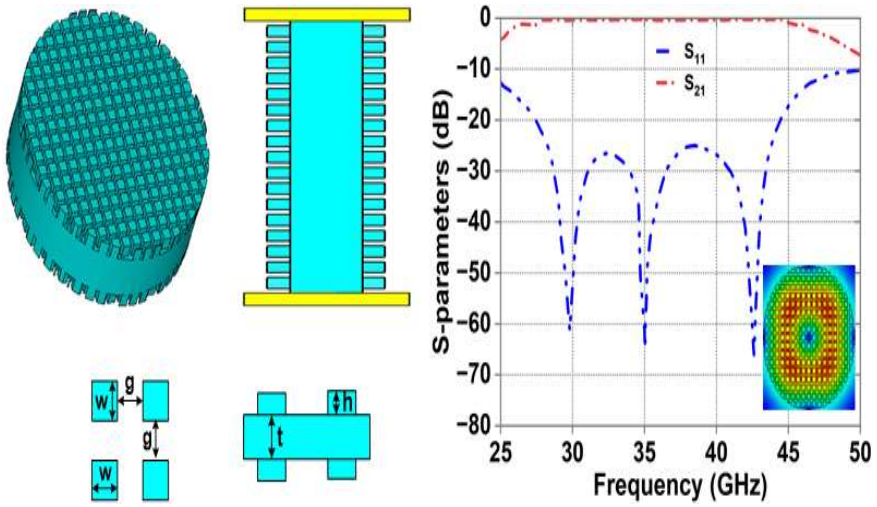

Fig. 6. 16. (a) Schematic diagram of Meta surface output window and **(b)** S-parameters.

The optimized design model of Meta surface window and E-field distribution of TE_{01} mode is shown in [Fig. 6. 16 (a)]. The S-parameters of the meta-surface window is shown in Fig. 6. 16 (b) the transmission and reflection losses are 0.22 dB and less than 20 dB over 15 GHz.

6.6. Conclusion

In the present chapter, the design of a multi-cavity stagger-tuned millimeter wave gyro-twystron working in the TE_{01} mode has been discussed. The proposed stagger-tuned gyrotwystron amplifier has greatly enhanced bandwidth while exhibiting minimum gain degradation. The interaction process between the RF wave and the electron beam of the current amplifier was investigated using self-consistent nonlinear theory, and the analytical results were confirmed using a commercially available 3D code (CST Particle-in-cell code). Using a stagger tuned approach, the device bandwidth increased by two times when compared to without a stagger tuning amplifier. Furthermore, a double anode MIG has been designed to generate a high-quality electron beam with a velocity spread of ~2% and a pitch factor of 1.4. To increase the efficiency of the amplifier, a multi-stage depressed collector was designed as the output

component. The current amplifier's overall efficiency rises from ~ 43% to ~78%. Finally, a Meta surface output window for collecting amplifier RF signal with wide bandwidth was designed, and its propagation characteristics were explored.